Analysis of the Internal Crazes in Notched SAN

E. S. SHIN, A. HILTNER,* and E. BAER

Department of Macromolecular Science and Center for Applied Polymer Research, Case Western Reserve University, Cleveland, Ohio 44106

SYNOPSIS

Crazing in styrene–acrylonitrile copolymer (SAN) under a triaxial stress state was examined. The damage zone that formed ahead of a semicircular notch under slow tensile loading consisted of two kinds of crazes: internal notch crazes that grew out from the notch root and discontinuous surface crazes. Examination of the damage zone in the optical and scanning electron microscopes revealed that the internal notch crazes sometimes extended through most of the thickness but never penetrated the free surfaces, whereas the surface crazes penetrated about 10–50 μm inward from the surface. Initially, the internal craze tips defined a crescent-shaped zone. The plane strain elastic stress distribution at the zone boundary satisfied a constant mean stress condition, and the critical mean stress for craze tip growth was determined to be about 35 MPa. This value varied slightly for different resins but was independent of thickness. Propagation of the internal notch crazes occurred in a straight line parallel to the minor principal stress vector at the point of origin on the notch surface, whereas the surface crazes followed the minor principal stress trajectories. The presence of the internal notch crazes resulted in significant stress redistribution, the stress redistribution was described quantitatively using both the deviation of the craze trajectory from the minor principal stress trajectory, and the deviation of the zone shape from the critical elastic mean stress condition.

INTRODUCTION

Irreversible prefracture deformation and damage of polystyrene (PS) and styrene–acrylonitrile copolymer (SAN), as with many brittle glassy polymers, is characterized by crazing. Several major reviews describe the complex nature of crazing, including such aspects as craze initiation and growth, craze structure and morphology, stress and environmental effects, temperature dependence, kinetics and viscoelastic behavior, and crazing in heterogeneous copolymers and blends.[1-4] The present understanding of the crazing phenomenon is based primarily on observations of crazing in thin films or of surface crazes in thicker sheet.

Crazing in a triaxial stress state is facilitated by use of a notched geometry. Deformation of some glassy amorphous polymers at a round notch has been comprehensively described by the initial formation of a plastic zone, followed by nucleation of an internal craze at the tip of the local plastic zone when a critical condition is achieved.[5-9] The craze initiation condition can be quantitatively described by slip line analysis of the plastic zone and related directly to fracture toughness. Under conditions where the craze initiation stress is smaller than the shear yield stress, a situation that might be achieved by varying the temperature, for example, crazes initiate at the notch root before shear yielding occurs and grow radially from the notch root.[10] This type of damage zone has not been as extensively studied.

The goal of this study was to characterize the nature of crazing in SAN under a triaxial stress state. A notched geometry was employed to create a triaxial stress state under uniaxial loading. The semicircular notch geometry is particularly attractive for studying prefracture damage since an exact numerical solution of the elastic stress field distribution over a fairly large region around the notch is available. Furthermore, the moderate stress intensifica-

* To whom correspondence should be addressed.

Journal of Applied Polymer Science, Vol. 46, 213–230 (1992)
 CCC 0021-8995/92/020213-18$04.00

tion and relatively smooth stress gradient at the notch tip minimize the tendency for premature brittle fracture. Finally, the semicircular notch geometry can be machined accurately while causing minimal predamage in the region of the notch root.

EXPERIMENTAL

Two SAN resins were used in this study: TYRIL 867-B (trademark of The Dow Chemical Co.) with 25% acrylonitrile (AN) by weight was supplied by Dow in the form of 1.1 mm-thick extruded sheet, and Lustran 31 (trademark of Monsanto Chemical Co.) with 25% AN by weight was obtained from Monsanto in the form of pellets. Specimens of various thicknesses were compression-molded from the Lustran in a preheated press at 200°C at 600 psi for 10 min and cooled slowly under pressure. Attenuated total reflection–Fourier transform infrared spectroscopy (ATR–FTIR) confirmed that the AN content in both SAN resins was the same.

Tensile tests of notched rectangular specimens 100×20 mm^2 were carried out on an Instron Testing Machine. A single 1 mm radius semicircular notch was machined midway along one edge using a sharp, high-speed steel end mill. The mill was air-cooled and only 0.1 mm was removed on each pass in order to minimize thermal effects and possible residual stresses at the notch surface. Some of the specimens from the extruded sheet were annealed at 105°C for 1 h after machining.

The damage zone at the notch was photographed during deformation with a traveling transmission optical microscope. Typically, photographs were obtained both with the focus on the surface and adjusted to the center of the thickness. A final magnification of 130× was achieved in the photographic prints used for analysis.

In some cases, specimens were loaded to specific positions on the stress-displacement curve and removed from the Instron for further characterization of the damage zone. For the optical microscope, a small section containing the damage zone was trimmed with a fine jewelry saw; the section was then microtomed to the desired depth in either the *xy* or *yz* plane. An RMC ultramicrotome (MT6000-XL) was used for this purpose.

For the scanning electron microscope (SEM), a procedure similar to that described in the literature was used.[11-14] A rectangular section 5×20 mm containing the damage zone was trimmed from the tensile specimen and cut through the center of the thickness with a low-speed, water-cooled Isomat diamond saw. The cut surface was polished on a polishing wheel with a fine grade of sandpaper and mounted on the SEM stage with a slight bend. The specimen was coated with about 90 Å of gold and viewed in the JEOL (JSM-840A). Fracture surfaces of notched tensile specimens were also examined in both the optical and scanning electron microscopes.

The optical micrographs were analyzed for the positions of the craze tips and for the craze trajectories. In both cases, the origin of the coordinate system was determined in each micrograph by selecting an *x*-axis about which the damage zone was symmetrical in both shape and direction. After the positions of the craze tips were determined in Cartesian coordinates, the local stresses were calculated using the appropriate equations. A four-step procedure was used to obtain the tangent to the craze line: (1) the craze lines were copied from the 130× optical micrographs onto transparent graph paper, (2) the coordinates of points every 2.5 mm along the craze line were determined using an optical microscope with a Graticule which gave a resolution of 0.01 mm, (3) the equation of the craze line was determined using nonlinear regression analysis, and (4) the first derivative of the equation at each point was taken to obtain the slope of the tangent.

RESULTS AND DISCUSSION

1. Damage Zone

The typical stress-displacement curve of notched 1.1 mm-thick SAN in uniform tension [Fig. 1(a)] was linear until catastrophic fracture. The points on the curve indicate the positions at which the photographs of the notch region in Figures 1(b)–(d) were obtained. The first damage was observed near the notch tip at a remote stress of about 20 MPa and consisted of discontinuous surface crazes that followed curved trajectories [Fig. 1(b)]. At a slightly higher stress, about 25 MPa, a second type of line damage was observed; this damage emanated from the notch surface and grew away from the notch as a family of continuous straight lines [Fig. 1(c)] at a remote stress of 33.6 MPa. This line damage was most clearly visible when the focus was adjusted to the center of the thickness and, consequently, was referred to as internal notch crazing. The damage zone defined by the internal notch crazes was initially crescent-shaped, but as the remote stress increased further, the damage zone acquired a triangular shape with the longest crazes in the center [Fig. 1(d)] at a remote stress of 40.7 MPa. With

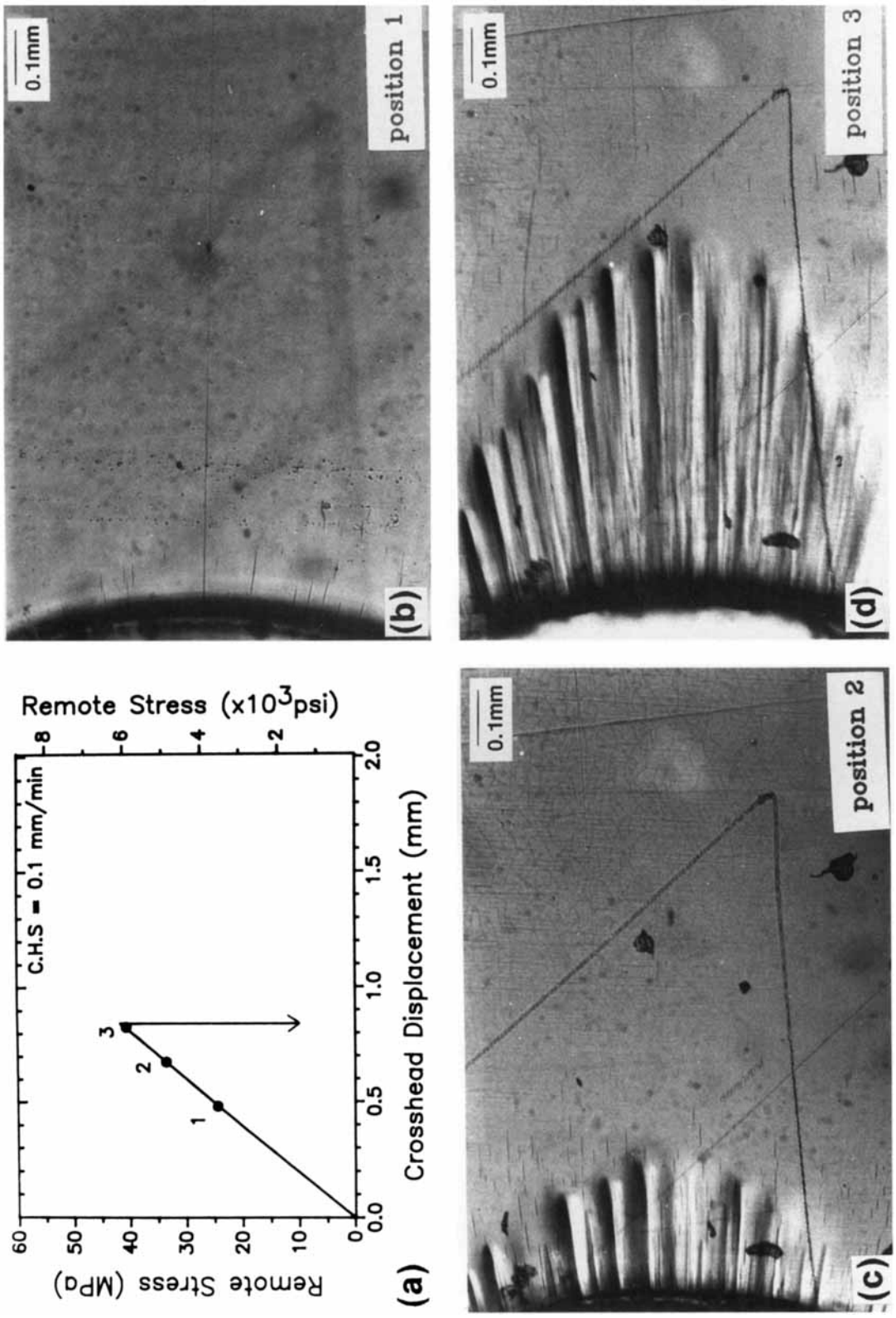

Figure 1 Tensile deformation of 1.1 mm-thick SAN with a semicircular notch: (a) the remote stress vs. displacement curve; (b) optical micrograph of the notch tip region at position 1 on the stress-displacement curve; (c) optical micrograph at position 2; (d) optical micrograph at position 3.

the relatively slow crosshead speed used in these experiments, 0.1 mm/min, the damage zone grew some distance away from the notch before fracture occurred catastrophically at a remote stress of 41.7 MPa for this particular specimen.

The crazelike microstructure of the internal line

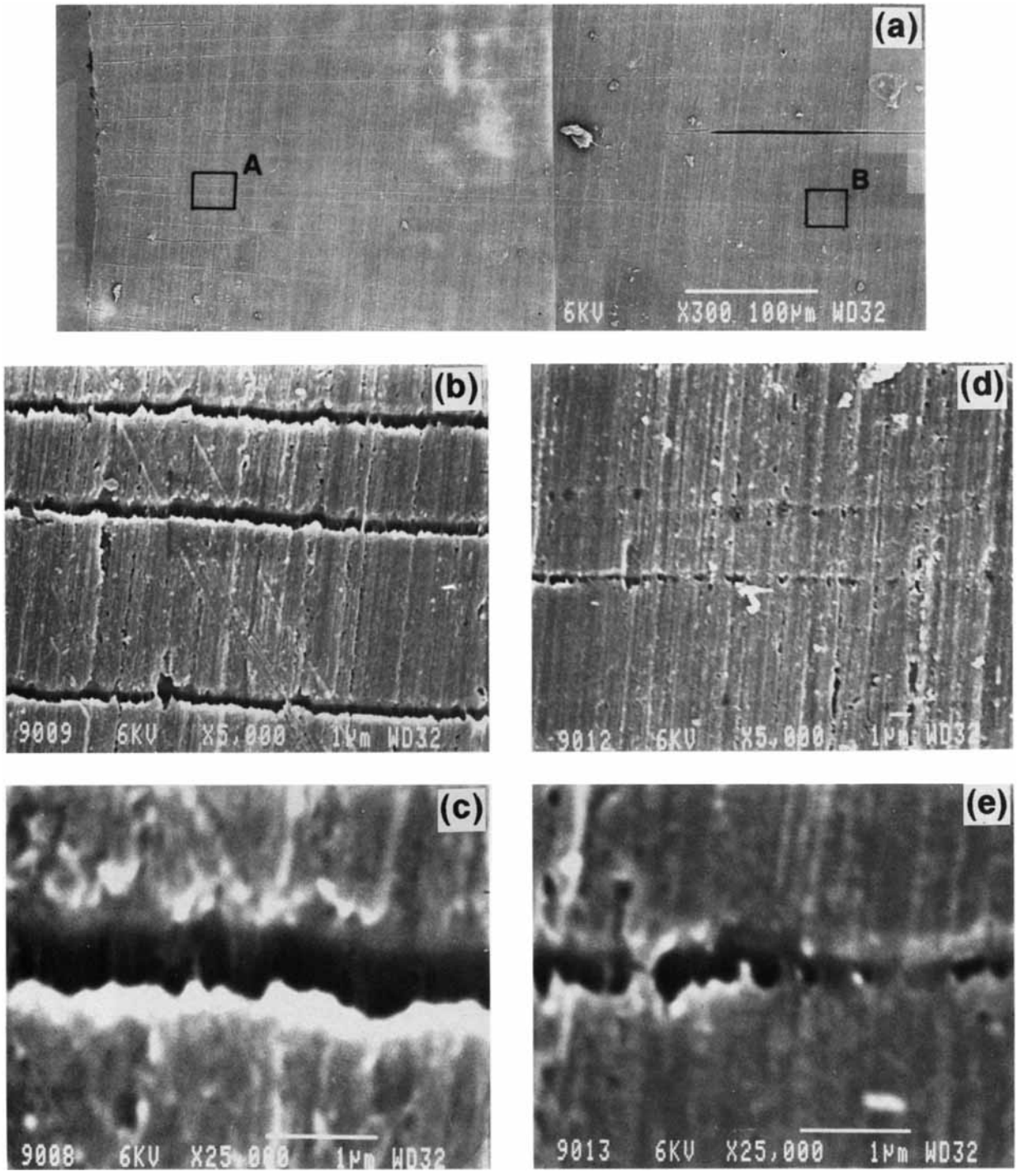

Figure 2 Scanning electron micrographs of the internal craze damage zone after the 1.1 mm-thick SAN was loaded to 35 MPa and sectioned in the *xy* plane through the center of the thickness: (a) low magnification view; (b, c) higher magnification views at position A; (d, e) higher magnification views at position B.

damage was confirmed by scanning electron microscopy. The low magnification micrograph in Figure 2(a) shows part of the damage zone of a specimen that had been loaded to 35.1 MPa and subsequently sectioned on the xy plane through the center of the thickness. During viewing in the SEM, the specimen was held under a slight bend; the small tensile load this created in the y direction opened up the damage lines to reveal the internal structure. Higher magnification micrographs of a pair of damage lines at the two positions identified in Figure 2(a), one near the notch [Fig. 2(b) and (c)] and the other at the tip of the lines [Fig. 2(d) and (e)], revealed microfibrils with diameters on the order of 50 nm and microvoids that are characteristic of the craze microstructure. There was no evidence even close to the notch to suggest that cracks had been initiated by fibril fracture; it appeared that prior to catastrophic fracture, fibrils spanned the crazes along their entire length, which enabled them to be load-bearing.

A microtomed cross section of the damage zone about 70 μm from the notch tip (Fig. 3) showed that the internal notch crazes often extended through most of the thickness. The discontinuous surface crazes were also visible in the cross section where they penetrated about 10–50 μm inward from both surfaces. Profiles of the internal notch crazes of a typical damage zone were constructed by locating each craze in successive cross sections, one of which is shown in Figure 3. The cross sections were separated by 20–50 μm and a total of 13 were used in the analysis. By drawing connecting lines through the positions of the craze tips in successive cross sections, the profiles in Figure 4 were obtained. In this figure, the point of craze initiation on the notch surface was identified by the perpendicular distance from the x-axis given by h (mm) = sin θ [insert, Fig. 4(a)]. Crazes in the center of the damage zone with growth planes close to the x-axis [Fig. 4(a)] included the longest crazes, but there were also numerous shorter crazes. Figure 4(b) shows crazes that were located midway between the x-axis and the edge of the damage zone, while those in Figure 4(c) were near the edge of the zone where the crazes were the shortest.

Although the craze length depended on the angle θ of the craze plane, it was characteristic that for any particular angle the maximum craze length did not vary through the thickness of the sheet. This suggested that the degree of triaxiality did not vary through the thickness and supported an assumption of the plane strain–stress state. In general, there was a wide range in both craze length and width. The internal notch crazes were able to grow in two directions and often were as wide or wider than they were long. Although they frequently grew very close to the free surface, they never penetrated it. This

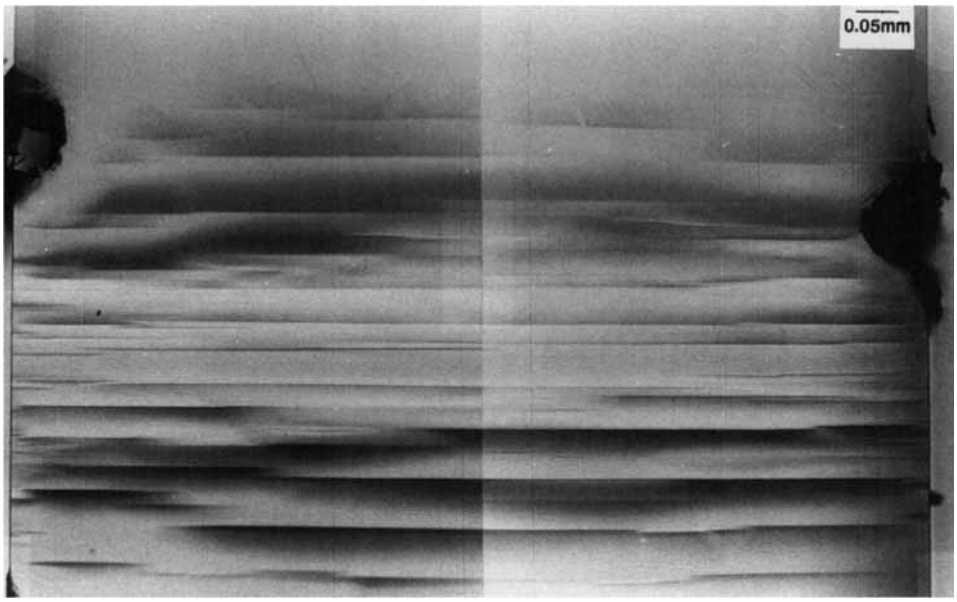

Figure 3 Microtomed cross section through the damage zone about 70 μm from the notch tip. The damage zone was created by loading the specimen to 37.9 MPa. The grooves on either side are markers to facilitate identification of individual crazes in sequential cross sections.

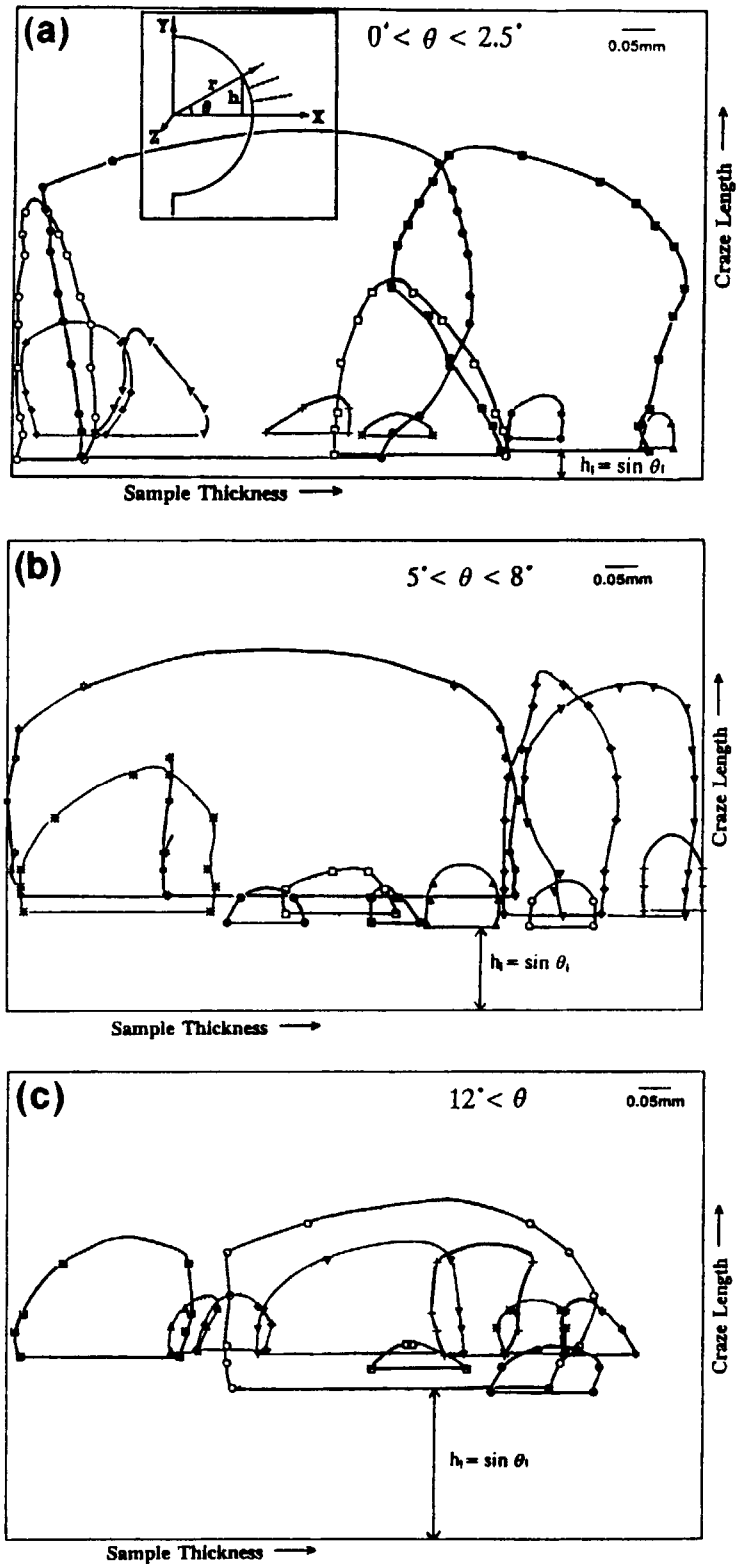

Figure 4 Profiles of internal notch crazes: (a) crazes in the center of the damage zone close to the x-axis (the insert shows the coordinate system used to locate the craze positions); (b) crazes located midway between the x-axis and the edge of the damage zone; (c) crazes near the edge of the damage zone.

feature of the internal notch crazes was confirmation that they initiated only from the notch surface, not from the free surface, and also suggested that their growth required some degree of triaxiality.

2. Condition for Internal Notch Craze Growth

The elastic stress field distribution was used in the analysis since the bulk glassy polymer could be treated as a linear elastic solid. Furthermore, because the crazes were load-bearing, it was assumed that they did not affect the stress distribution significantly when the damage zone was small. The elastic stress field distribution of a single-edge semicircular notched body published previously[15] was derived from Maunsell's exact numerical solution.[16] From the stress field equations for the two-dimensional stress state, $\sigma_{ij} = f(\sigma_0, r, \theta)$, the principal stresses σ_1 and σ_2 were obtained from classical continuum mechanics relationships:

$$\sigma_{\max}, \sigma_{\min} = \sigma_1, \sigma_2 = \frac{\sigma_{rr} + \sigma_{\theta\theta}}{2} \pm \sqrt{\left(\frac{\sigma_{rr} - \sigma_{\theta\theta}}{2}\right)^2 + \sigma_{r\theta}^2} \quad (1)$$

and in the case of plane strain,

$$\sigma_m = \frac{\sigma_{rr} + \sigma_{\theta\theta} + \sigma_{zz}}{3} = \frac{\sigma_1 + \sigma_2 + \sigma_3}{3} \quad (2)$$

where $\sigma_3 = \nu(\sigma_1 + \sigma_2)$. The resulting isostress contours, normalized to the remote stress, are plotted with the major and minor principal stresses in Figure 5(a) and the mean stress in Figure 5(b). The maximum normalized value of σ_1 was 3.06 at the notch tip, whereas that of σ_2 was 0.413 and was located 0.47 mm from the notch tip on the x-axis. The maximum normalized mean stress depended on the Poisson's ratio and for $\nu = 0.35$, a typical value for SAN,[17] was equal to 1.375 at the notch root.

The positions of the internal notch craze tips are plotted in Figure 6 for several values of the remote stress. The locus of these points, particularly for the lower stresses, defined a crescent shape that resembled both the σ_1 and σ_m contours, suggesting that a constant stress condition characterized the damage zone boundary. To distinguish between the two possibilities, values of σ_1 and σ_m at the tip of each internal notch craze were plotted as a function of the angle θ for six damage zones from three different experiments (Fig. 7). The positions of the craze tips fit a constant σ_m condition, and for this SAN resin, the critical mean stress for internal craze growth $\sigma_{m,c}$ was 35.1 MPa. The standard deviation in $\sigma_{m,c}$ values from a single damage zone was about 5%, and for the data from all six zones, was about 8%. On the other hand, the major principal stress exhibited a decreasing trend from the edge of the zone to the center with an overall variation of about 15%. The observation that the position of the internal notch craze tips was determined by a mean stress condition

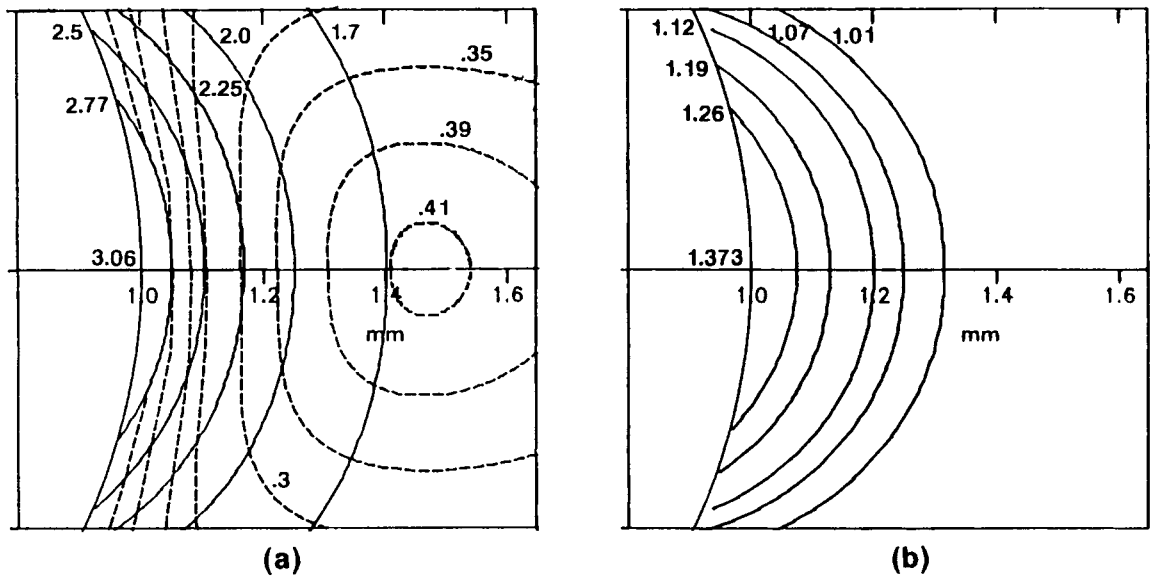

Figure 5 Normalized isostress contours: (a) major principal stress (solid lines) and minor principal stress (dashed lines); (b) mean stress.

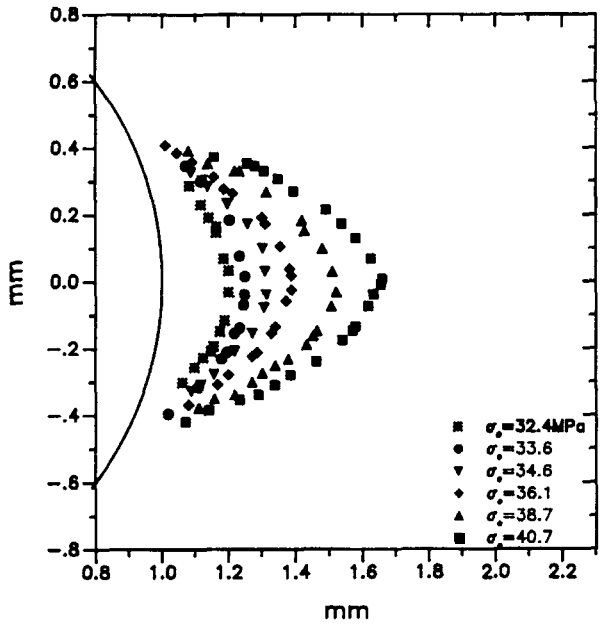

Figure 6 Positions of the internal notch craze tips for several remote stresses.

derived from the plane strain state suggested that cavitation was the controlling microdeformation mechanism in the craze growth process.

Stress-whitening of PVC blends with chlorinated polyethylene (CPE) impact modifier also produces a crescent-shaped damage zone ahead of a semicircular notch that is described by a constant mean stress.[15] In this case, the corresponding elastic volume strain V_c was calculated by

$$V_c = \frac{\sigma_{m,c}}{K} = \frac{3(1-2\nu)\sigma_m}{E} \tag{3}$$

where K is a bulk modulus; and E, Young's modulus. Because V_c was independent of temperature, the amount of CPE in the blend, and also the physical properties of the CPE, it was suggested that in this instance the critical condition for cavitation is a volume strain. It has also been suggested that crazing of polycarbonate follows a critical volume strain condition.[18] The value of V_c for SAN obtained from $\sigma_{m,c}$ was 0.95, in the same range as that of PVC (0.8) and PC (1.2).

On the other hand, several well-known theories of craze growth are based on stress criteria. In the meniscus instability model,[19,20] craze growth is controlled by the principal stress σ_1. Two other fracture mechanics approaches also predict a critical principal stress condition for craze growth.[21,22] Other models require a dilational mean stress condition, including the stress-activated devitrification hypothesis[23,24] and an isolated void mechanism[25] that is supported by recent experimental observations.[26] There is presently no agreement on a single model; in fact, there may be more than one mechanism of

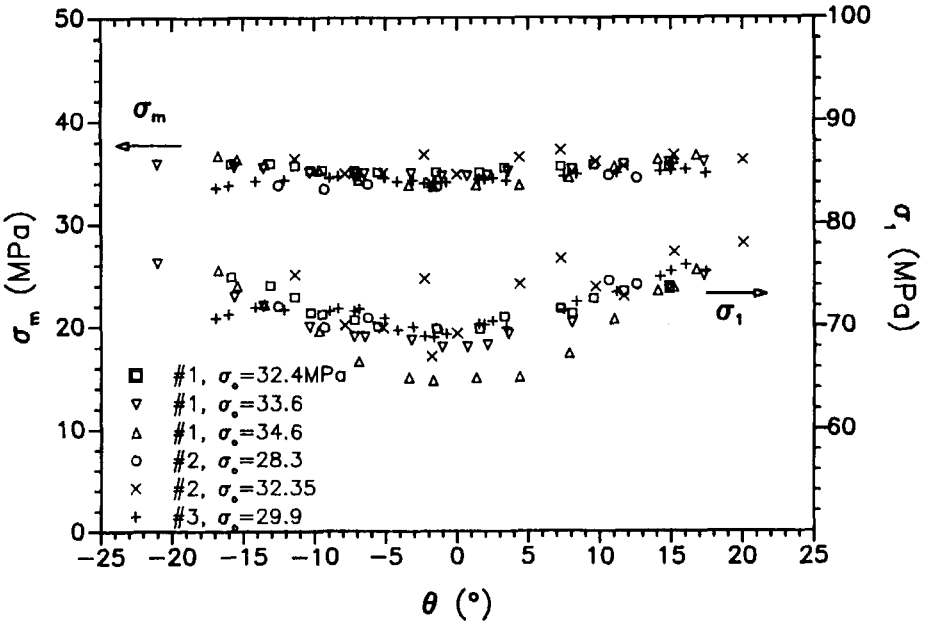

Figure 7 Mean stress (σ_m) and major principal stress (σ_1) at the positions of the craze tips for lower remote stresses as a function of the angle θ.

craze growth and the most appropriate model may therefore depend on the particular polymer and experimental conditions. In the present case, growth of internal notch crazes in SAN was more closely described by a dilational mean stress condition than by a principal stress condition.

3. Mean Stress Redistribution

The shape of the damage zone conformed best to the mean stress condition at the lower remote stresses. Although the average value obtained for $\sigma_{m,c}$ did not change as the remote stress increased, the standard deviation was larger and some curvature was apparent in the dependence of σ_m on θ. This reflected a change in shape of the damage zone as the presence of the internal notch crazes began to significantly affect the stress distribution around the damage zone. It is well known that when crazing is profuse the stress distribution, and thus the craze propagation behavior, is affected.[27,28] To magnify the effect of stress redistribution, which could not be easily discerned in Figure 7, it was assumed that craze growth was controlled by the mean stress condition at all remote stress levels and the deviation from the elastic stress distribution was characterized. The mean stress deviation, $\Delta\sigma_m$, was defined as the difference between $\sigma_{m,c}$, the mean stress calculated from the craze tips when the zone was small, which was equal to 35.1 MPa for this resin, and $\sigma_{m,E}$, the apparent elastic mean stress at the craze tip if stress redistribution were neglected, which was calculated from eq. (2).

The stress redistribution resulted in the zone becoming increasingly longer than the reference along the x-axis, $\theta = 0$, and increasingly shorter at the edges. The trend became more pronounced as the remote stress increased. Normalized values of $\Delta\sigma_m$ are plotted in Figure 8 as a function of the angle θ for several remote stresses. The degree of redistribution was highest at $\theta = 0°$, decreased with increasing angle θ to zero at about $\theta = 11°$, and became increasingly negative toward the edges. A cross-plot of the data from Figure 8 showed that the normalized quantity $\Delta\sigma_m/\sigma_{m,E}$ increased linearly with the remote stress at all angles and the slope depended on θ and ranged from about 0.0127/MPa at $\theta = 0°$ to about -0.011/MPa at $\theta = \pm 20°$. By extrapolation of the linear dependence to $\Delta\sigma_m/\sigma_{m,E} = 0$, it was estimated that stress redistribution started to affect the shape of the damage zone at a remote stress of about 31 MPa. This compared with a remote stress for the beginning of damage zone growth of 25.5 MPa, which was estimated from $\sigma_{m,c}$ (35.1 MPa) and the elastic mean stress concentration factor. The value 25.5 MPa was also close to the stress at which the internal notch crazes were first observed with a traveling optical microscope. Together, these two

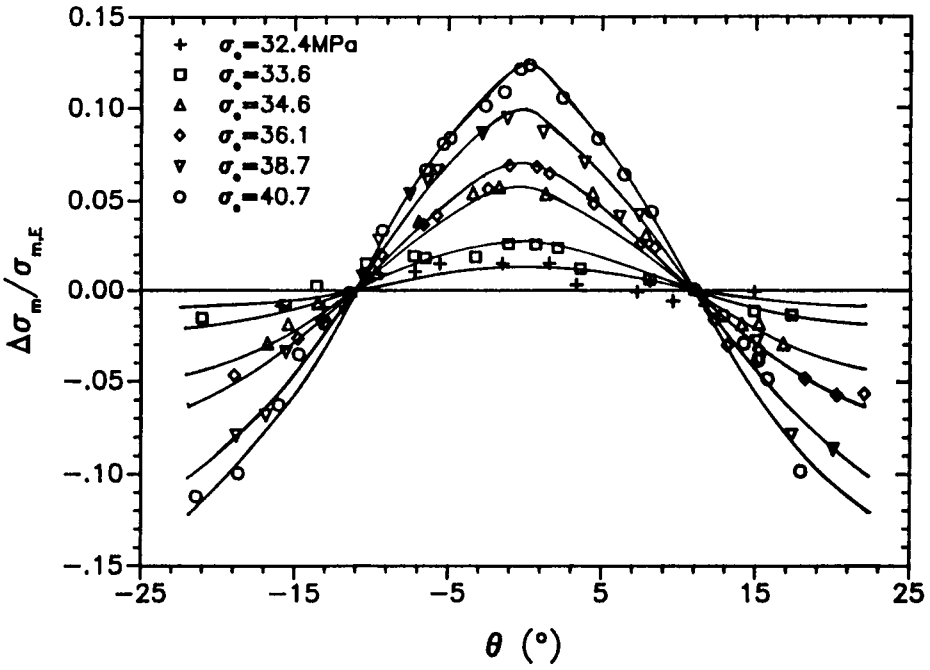

Figure 8 The normalized mean stress deviation at the positions of the internal notch craze tips.

values, 25.5 and 31 MPa, defined the range in remote stress over which the elasticity equations adequately described the stress distribution at the boundary of the damage zone.

There are several possible explanations for deviation in the positions of the craze tips from the mean stress condition. Stress intensification at the craze tip would cause the craze length to exceed the length determined by the mean stress condition. This effect would be most pronounced where the $\sigma_{m,c}$ condition requires the crazes to be longest, at $\theta = 0°$, since the stress intensification is proportional to the square root of the craze length.[29] On the other hand, overlapping stress fields can retard craze growth.[27] The cumulative effect of stress or strain release in neighboring crazes would be most pronounced where the crazes are initially the shortest, that is, those at the largest θ angles. The two effects would tend to reinforce each other so that crazes at small θ would become increasing longer and crazes at large θ increasingly shorter than the mean stress condition as the remote stress increased. In this case, the result was actually symmetrical about an angle $\theta = 11°$.

4. Elastic Stress Trajectories

It is well established that surface crazes in glassy polymers generally follow the minor principal stress trajectories.[30-32] Furthermore, the elastic stress trajectories closely describe the crazes for many notch geometries including the sharp notch, various angled notches, and the circular hole. The stress trajectories can be obtained experimentally from photoelasticity[33] or analytically from the principal stress vectors.[32] The trajectories are continuous and differentiable, and by definition, the stress vector is tangent to the trajectory so that at every point the direction of the stress vector and the trajectory are the same.

The directions of the principal stress vectors at a given position are given by the relationship

$$\tan 2\gamma = \frac{2\sigma_{r\theta}}{\sigma_{rr} - \sigma_{\theta\theta}} \tag{4}$$

where γ is the angle between the principal stress direction and the x-axis. The elastic stress field equations of Maunsell were used to obtain the vectors of the minor and major principal stresses at and near the notch surface. The minor principal stress vectors were directed radially from the origin of the coordinate system at the notch surface and gradually curved away from the notch, eventually becoming perpendicular to the loading axis.

The trajectories were obtained from the stress vectors as follows: At a given position on the notch (x_1, y_1), the vector of the minor principal stress was obtained using eq. (4). This was the starting point of the trajectory. A second point (x_2, y_2) was chosen

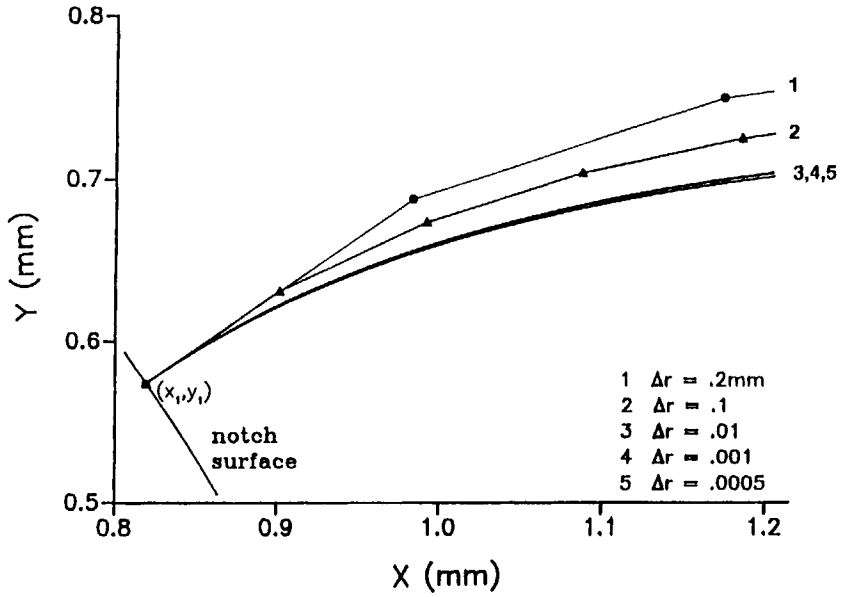

Figure 9 Representation of the principal stress trajectory in terms of the increment Δr.

as the incremental distance $\Delta r = \{(x_2 - x_1)^2 + (y_2 - y_1)^2\}^{1/2}$ along the vector and the minor principal stress direction calculated again at this new position: (x_2, y_2). The process was repeated again at (x_3, y_3), and so on. When the increment Δr was small enough, an accurate trajectory was obtained by this method. The trajectories calculated for several values of Δr are shown in Figure 9; no significant changes were observed when the increment was smaller than 0.01 mm. For the purposes of this analysis, Δr was chosen to be 0.0005 mm.

5. Craze Trajectories

Profuse surface crazing was produced by applying a crazing agent, machine oil, to the surface. In this

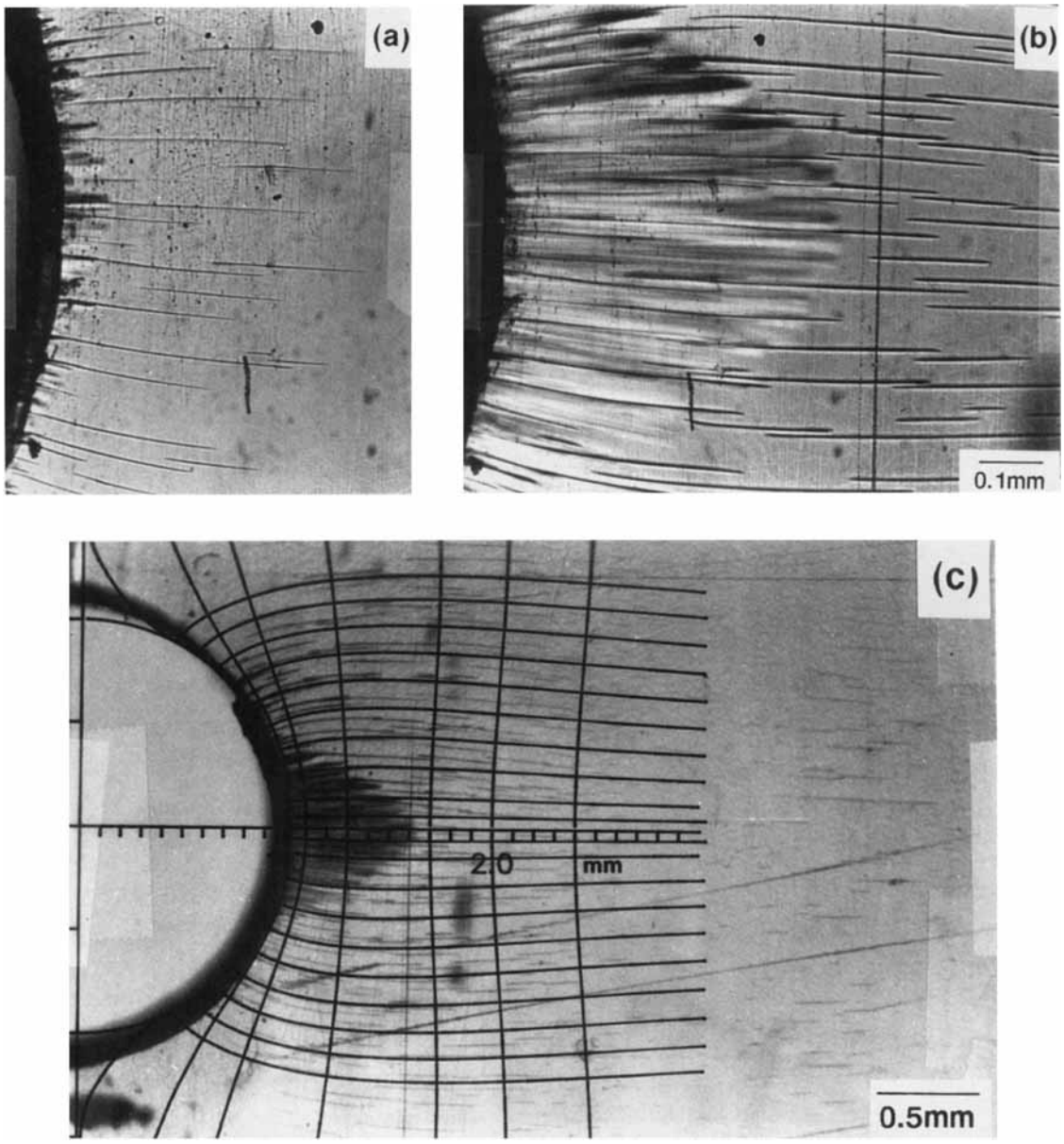

Figure 10 Surface crazes produced with machine oil: (a) optical micrograph of the notch region loaded to 31.8 MPa; (b) optical micrograph at 36.0 MPa; (c) lower magnification optical micrograph at 36.8 MPa with the major and minor principal stress trajectories superimposed.

case, surface crazes originated from the notch at a remote stress of about 20 MPa. These crazes, together with some secondary surface crazes, are shown at a somewhat higher stress, 31.8 MPa, in Figure 10(a). The focus was on the surface in order to view the surface crazes, but the beginning of the small, crescent-shaped internal craze zone was also apparent in the micrograph. The secondary surface crazes became more numerous at 36 MPa [Fig. 10(b)] and extended further from the notch; the multiple internal crazes that composed the out-of-focus crescent-shaped zone had also lengthened. The region ahead of the notch is shown again in Figure 10(c) after the remote stress was increased to 36.8 MPa. A lower magnification was used and the elastic principal stress trajectories were superimposed to demonstrate that growth of both primary and secondary surface crazes conformed to the curved σ_2-trajectories.

Multiple internal notch crazes that differ from surface crazes by following linear trajectories have previously been observed in thick notched specimens of various other polymers.[10,14,34,35] The xy section through the internal notch craze zone in Figure 11 was obtained by sectioning a specimen through the center of the thickness after it had been loaded to 35 MPa. Superimposed are the major and minor principal stress vectors at the positions on the notch where the internal notch crazes initiated. It is clear that growth of the internal notch crazes followed the straight line defined by the σ_2-vector at the point of initiation on the notch.

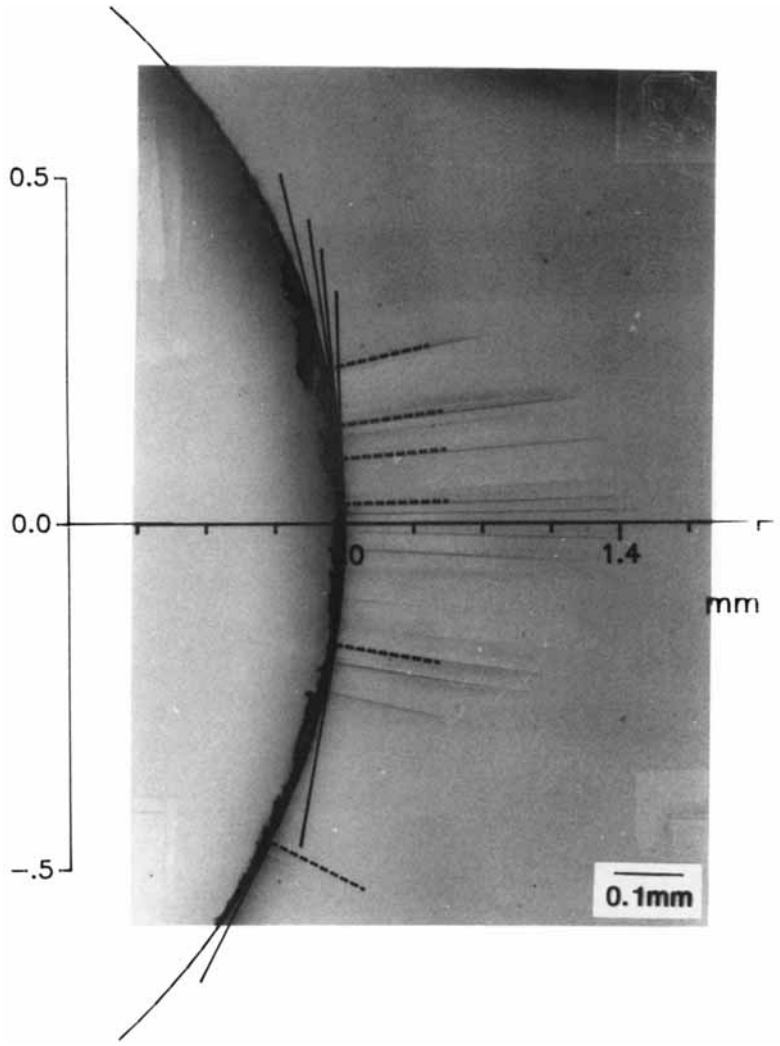

Figure 11 Microtomed section in the xy plane through the center of the thickness. The damage zone was created by loading the specimen to 35.0 MPa. The vectors of the principal stresses at the position of craze initiation on the notch surface are superimposed.

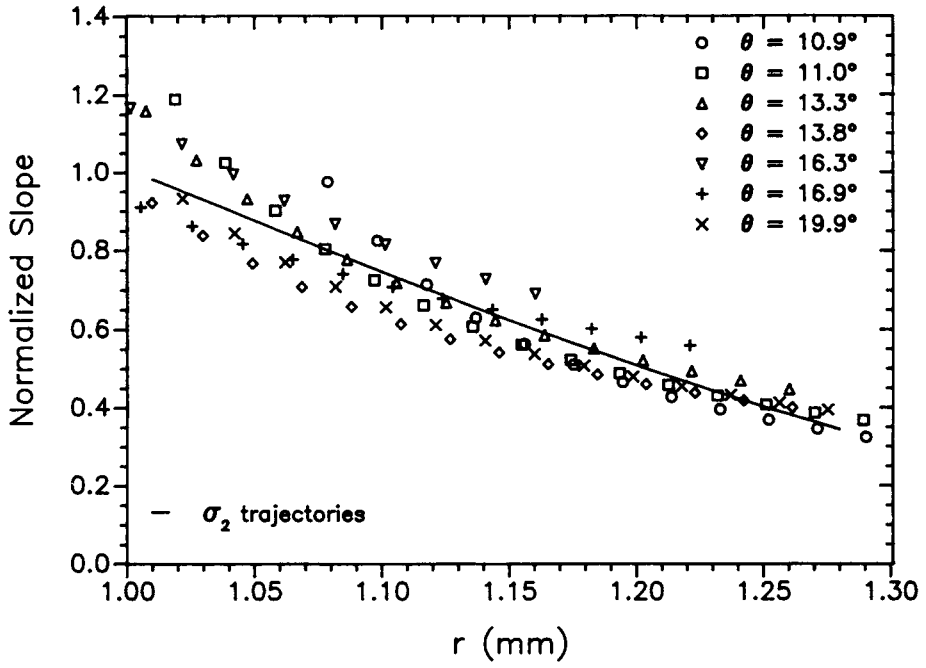

Figure 12 The normalized slope of several surface crazes compared with the calculated normalized slope of the σ_2-trajectories.

To quantify the relationship between craze growth direction and the elastic stress distribution, the craze slopes, defined as the slope of the tangent to the craze line at any point on the craze, were compared with the slopes of the σ_2-trajectories. The calculated slope of the σ_2-trajectory was virtually independent of θ over the range of interest, $|\theta| \leq 20°$ and $r \leq 1.3$ mm, when normalized to tan θ, the slope

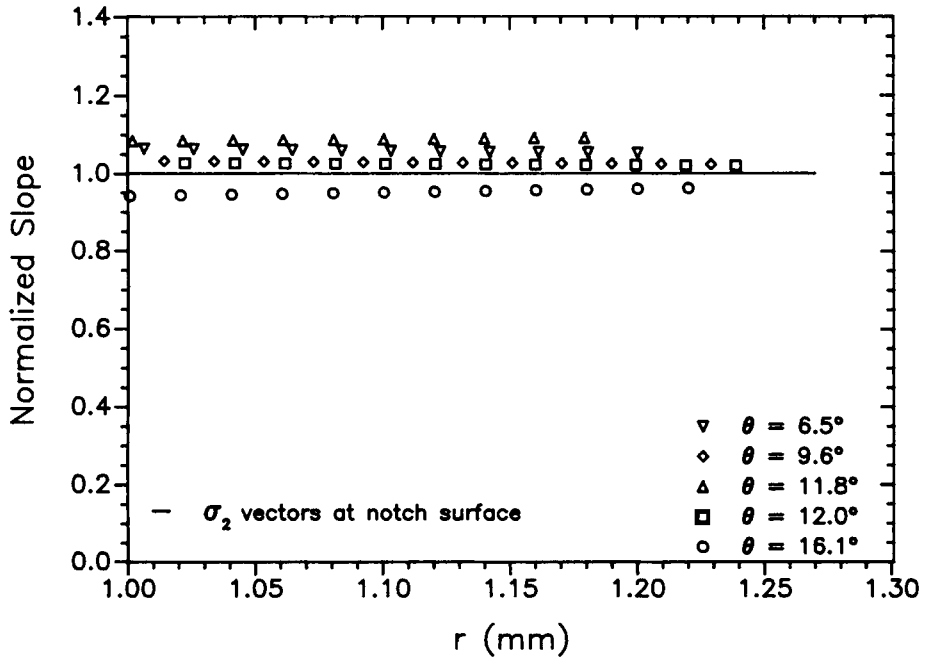

Figure 13 The slope of several internal notch crazes normalized to the slope of the σ_2-vector at the position of craze initiation on the notch surface.

Table I Conditions for the Craze Tip Growth

Sample Thickness	$\sigma_{m,c}$ (MPa)	V_c (%)
1.1 mm (TYRIL)	35.1 ± 2.0	0.95
1.1 mm (TYRIL) annealed	35.5 ± 1.5	0.96
3.1 mm (Lustran)	31.2 ± 1.2	0.84
1.1 mm (Lustran)	32.5 ± 1.5	0.87
0.6 mm (Lustran)	30.5 ± 1.0	0.82
0.5 mm (Lustran)	32.3 ± 1.0	0.87

at the starting position of the trajectory on the notch surface. The calculated normalized slope, represented by the solid line in Figure 12, decreased gradually from unity as the trajectories curved away from the notch surface. Values obtained for the normalized slope at a number of points along several surface crazes are also included in Figure 12. Crazes were selected from optical micrographs obtained at various remote stresses in order to make certain that the craze direction was not affected significantly by the small notch opening at the higher stresses. Furthermore, only crazes that initiated at positions described by larger θ angles were analyzed since both craze trajectories and minor principal stress trajectories were nearly parallel to the x-axis when θ was within ± 10°. The correspondence in Figure 12 shows that the surface crazes followed the σ_2-trajectories.

The normalized slope of several internal notch crazes is compared with unity in Figure 13. The craze slopes were normalized to tan θ at the position where the craze originated on the notch surface, and unity corresponded to the normalized slopes of the σ_2-vectors at the notch surface. The linearity of the internal notch crazes was apparent from the constant values of the normalized slope. However, the crazes did not always initiate perpendicular to the notch surface, probably because of irregularities in the machined notch, and this accounted for values of the normalized slope that were constant but different from unity for certain crazes. The difference between growth behavior of surface and internal crazes was clear from a comparison of Figures 12 and 13; the growth directions of the former closely followed the σ_2-trajectories, while growth of the latter proceeded in the direction defined by the σ_2-vector at the position of craze initiation on the notch.

6. Effect of Thickness

The assumption that the internal notch crazes grew in a plane strain–stress state was tested by varying the thickness of specimens molded from the Lustran resin. A damage zone created by internal notch

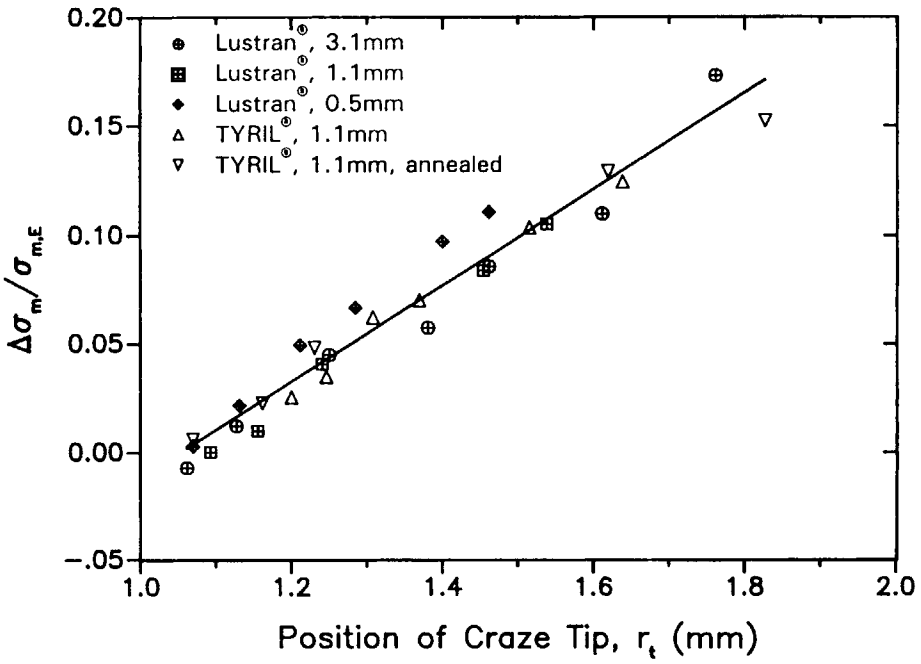

Figure 14 The normalized mean stress deviation at the positions of the internal notch craze tips at $\theta = 0°$ for various SAN samples.

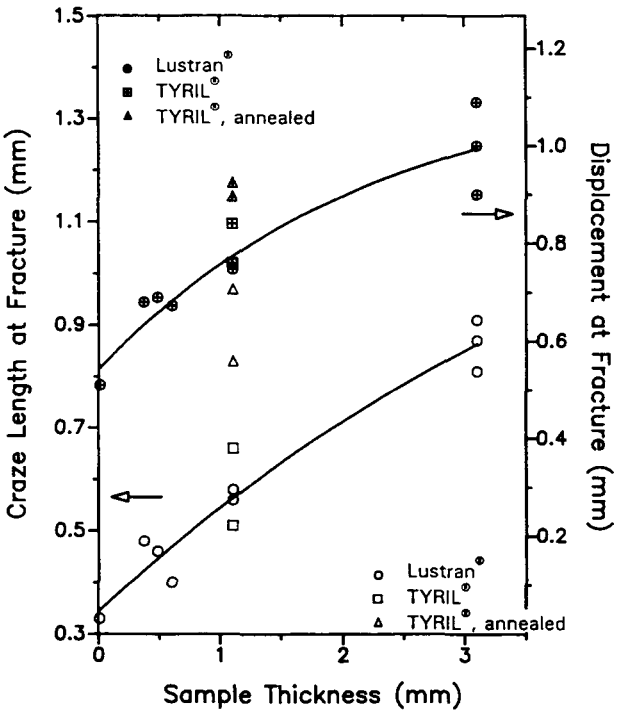

Figure 15 Maximum length of the damage zone of the internal notch crazes at fracture as a function of sample thickness. Macroscopic remote displacement at fracture is also plotted for different SAN samples.

crazes was observed in notched specimens with thicknesses of 3.1, 1.1, 0.5, and 0.01 mm; except for the 0.01 mm thin film that fractured after the first few crazes formed, the zone defined by the craze tips was described by a constant mean stress condition. The value obtained for $\sigma_{m,c}$ was, within experimental error, independent of thickness (Table I). At 31.6 MPa, the average value of $\sigma_{m,c}$ for the Lustran resin was slightly higher than that obtained for the extruded TYRIL sheet: 35.1 MPa; the small difference might have resulted from differences in the resins or from residual effects of processing.

At higher stresses, the shape of the zone defined by the craze tips deviated from the constant σ_m crescent shape in essentially the same way for all the thicknesses examined with the exception of the thin film that fractured before enough crazes had formed to define a damage zone. The similarity was demonstrated by comparing the normalized mean stress deviation $\Delta\sigma_m/\sigma_{m,E}$ at $\theta = 0°$. In all cases, the same linear dependence on the remote stress was observed (Fig. 14). In general, the length that the damage zone achieved before catastrophic fracture increased as the thickness increased with a corresponding increase in the macroscopic remote displacement at fracture (Fig. 15). Annealing also resulted in an increase in the length of the damage zone.

7. Fracture

Catastrophic fracture occurred when the internal craze zone reached a critical length that depended on the thickness. Bifurcation was always observed (Fig. 16), a phenomenon that is frequently observed in conjunction with high-velocity, brittle fracture of glassy polymers. It has been suggested that bifur-

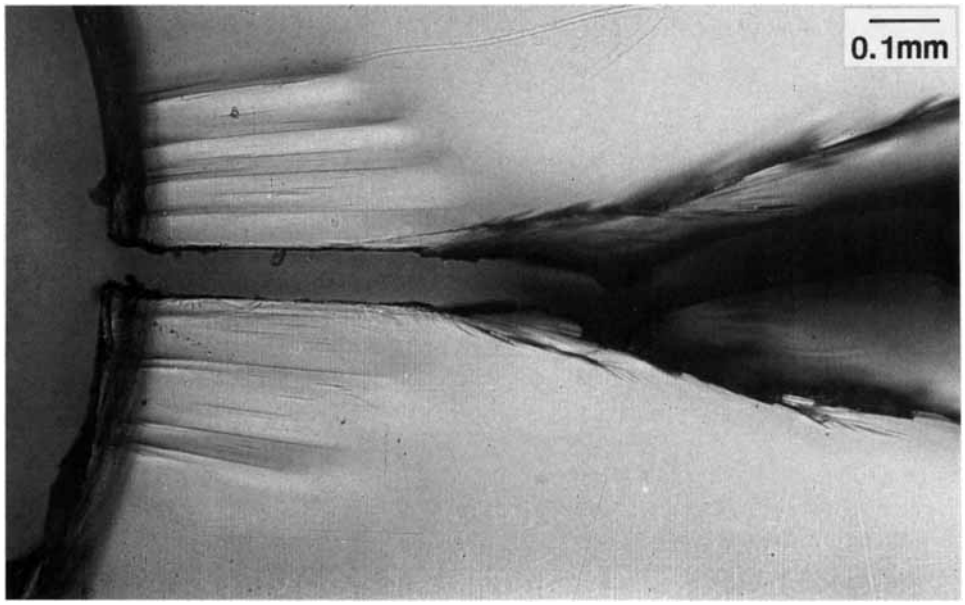

Figure 16 Optical micrograph of the fractured 1.1 mm-thick SAN sample.

Figure 17 Optical micrograph of fracture surface of 1.1 mm-thick SAN sample.

cated crack growth in homogeneous glassy polymers is a consequence of the stress redistribution that occurs at the tip of the rapidly moving crack.[36,37]

The corresponding fracture surface (Fig. 17) showed the features typical of brittle glassy polymers such as polystyrene[38,39] and poly(methyl methacrylate).[37] Three distinct regions were distinguishable on the fracture surface: a textured region abutting the notch surface where crack initiation occurred; a smooth mirror region of faster crack growth that surrounded the initiation region and extended the length of the preexisting damage zone, about 0.6 mm from the notch for the 1.1 mm-thick sheet; and an irregular, banded hackle region further from the notch.

These features of the fracture surface are related to the processes that accompany crack propagation in crazing materials.[40] The crack initiated by cavitation of the preformed craze and propagated along the center of the craze by tearing of the fibrous material in the craze layer. Secondary fracture features gave the initiation region its characteristic texture [Fig. 18(a)]. As the crack continued to propagate through the preformed crazes of the damage zone, the mode of crack propagation changed as the velocity increased. Splitting along the interface between crazed and uncrazed material created the smooth mirrored appearance that characterized the remainder of the precrazed region. At higher magnification, small islands of material were seen in this region of the fracture surface where the crack jumped from one interface to the other [Fig. 18(b)]. These markings are referred to as mackerel or patch patterns depending on whether they are regular or irregular.[38] The solid dark bands through the mirror region suggested that occasionally the crack also jumped from one craze to another as it propagated. The hackle pattern was observed when the crack passed beyond the tip of the damage zone and propagated through initially uncrazed material. The hackle resulted when the crack nucleated a set of crazes close to its tip and then propagated along one of these crazes. Rapid propagation allowed the stress to relax locally and the crack slowed enough for a new set of crazes to form at the new position. Repetition of this process caused the crack to propagate by jumps and created the characteristic banding of the hackle pattern.[41]

CONCLUSIONS

The nature of crazing in SAN under a triaxial stress state has been studied. Analysis of the damage zone that formed at a semicircular notch during slow tensile loading led to the following conclusions:

1. The damage zone is composed of continuous internal notch crazes and discontinuous surface crazes. The internal notch crazes grow in two directions but never penetrate the free surfaces, while the surface crazes penetrate about 10–50 μm inward.
2. Initially, the internal craze tips define a crescent-shaped zone. The plane strain elastic stress distribution at the zone boundary in-

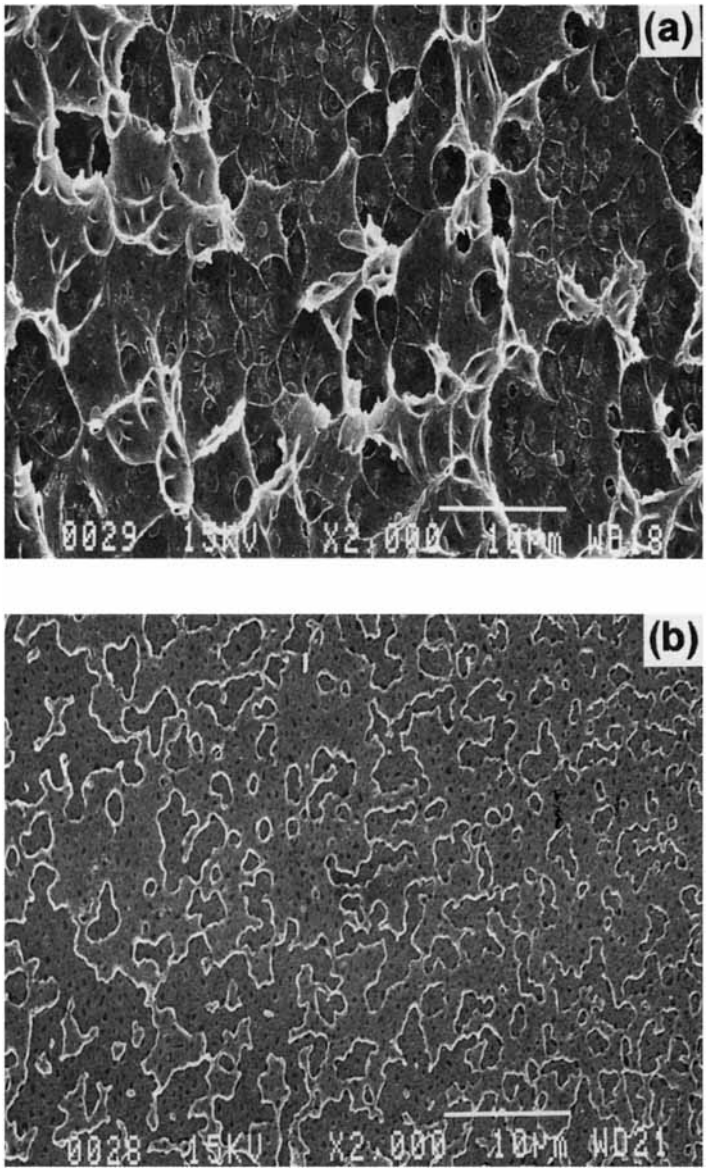

Figure 18 Scanning electron micrographs of fracture surface of 1.1 mm-thick SAN sample: (a) high-magnification view at position a in Figure 17; (b) high-magnification view at position b in Figure 17.

dicates that internal craze tip growth is described by a critical mean stress condition.

3. The internal notch crazes propagate in a straight line parallel to the minor principal stress vector at the point of origin on the notch surface while the surface crazes follow the minor principal stress trajectories.
4. Stress redistribution associated with the internal notch crazes is significant and can be described quantitatively using either the deviation of the craze trajectory from the minor principal stress trajectory or the deviation of the zone shape from the critical elastic mean stress condition.

This research was generously supported by The Dow Chemical Company, Midland, MI, and the National Science Foundation, Polymers Program (DMR 9100300).

REFERENCES

1. S. Rabinowitz and P. Beardmore, *CRC Rev. Macromol. Sci.*, **1**, 1 (1972).
2. R. P. Kambour, *J. Polym. Sci. Macromol. Rev.*, **7**, 1 (1973).

3. H. H. Kausch, Ed., *Adv. Polym. Sci.*, **52/53** (1983).
4. H. H. Kausch, Ed., *Adv. Polym. Sci.*, **91/92** (1990).
5. N. J. Mills, *J. Mater. Sci.*, **11,** 363 (1976).
6. M. Ishikawa, I. Narisawa, and H. Ogawa, *J. Polym. Sci. Polym. Phys. Ed.*, **15,** 1791 (1977).
7. I. Narisawa, M. Ishikawa, and H. Ogawa, *J. Mater. Sci.*, **15,** 2059 (1980).
8. M. Ishikawa, H. Ogawa, and I. Narisawa, *J. Macromol. Sci.-Phys.*, **B19**, 421 (1981).
9. M. Kitagawa, *J. Mater. Sci.*, **17,** 2514 (1982).
10. M. Kitagawa and H. Yammaura, *J. Mater. Sci.*, **19,** 1863 (1984).
11. M. Dettenmaier and H. H. Kausch, *Polymer*, **21,** 1232 (1980).
12. W. Doll, *Adv. Polym. Sci.*, **52/53**, 105 (1983).
13. B. Z. Jang, D. R. Uhlmann, and J. B. Vander Sande, *Polym. Eng. Sci.*, **25**, 98 (1985).
14. I. Narisawa and M. Ishikawa, *Adv. Polym. Sci.*, **91/92,** 353 (1990).
15. A. Tse, E. Shin, A. Hiltner, and E. Baer, *J. Mater. Sci.*, **26,** 2823 (1991).
16. F. G. Maunsell, *Philos. Mag.*, **21,** 765 (1936).
17. J. Im, E. Baer, and A. Hiltner, in *High Performance Polymers,* E. Baer and A. Moet, Eds., Hanser, New York, 1991, p. 175.
18. R. P. Kambour, M. A. Vallance, E. A. Farraye, and L. A. Grimaldi, *J. Mater. Sci.*, **21,** 2435 (1986).
19. A. S. Argon and M. Salama, *Philos. Mag.*, **36**, 1217 (1977).
20. A. M. Donald and E. J. Kramer, *Philos. Mag., A,* **43**, 857 (1981).
21. A. C. Knight, *J. Polym. Sci. A,* **3,** 1845 (1965).
22. N. Verheulpen-Heymans and J. C. Bauwens, *J. Mater. Sci.*, **11,** 1 (1976).
23. A. N. Gent, *J. Mater. Sci.*, **5,** 925 (1970).
24. A. N. Gent, *J. Macromol. Sci.-Phys.*, **B8**, 597 (1973).
25. A. S. Argon, *J. Macromol. Sci.-Phys.*, **B8**, 573 (1973).
26. G. H. Michler, *Colloid Polym. Sci.*, **264,** 522 (1986).
27. A. Moreno and E. Baer, in *Structure-Property Relationships of Polymeric Solids,* A. Hiltner, Ed., Plenum Press, New York, 1983, p. 1.
28. P. Beardmore and S. Rabinowitz, *J. Mater. Sci. Lett.*, **6,** 80 (1971).
29. J. G. Williams, *Stress Analysis of Polymers,* Wiley, New York, 1973.
30. S. Sternstein, L. Ongchin, and A. Silverman, *Applied Polymer Symposia,* No. 7, Interscience, New York, 1968, p. 175.
31. M. Bevis and D. Hull, *J. Mater. Sci.*, **5,** 983 (1970).
32. M. Chabaat, *Int. J. Fracture* **37,** R47 (1988).
33. D. Post, *Proc. Soc. Exp. Stress Anal.*, **12,** 99 (1954).
34. M. Ishikawa and I. Narisawa, in *Proceedings of the 25th Japan Congress on Materials Research,* Kyoto, Japan, 1982, p. 282.
35. L. H. Lee, J. F. Mandell, and F. J. McGarry, *Polym. Eng. Sci.*, **27**, 1128 (1987).
36. E. H. Yoffe, *Philos. Mag.*, **42,** 739 (1951).
37. B. Rosen, *Fracture Processes in Polymeric Solids,* Interscience New York, 1964, Chap. II.
38. J. Murray and D. Hull, *J. Polym. Sci. A-2,* **8,** 1521 (1970).
39. J. A. Sauer and C. C. Chen, *Adv. Polym. Sci.*, **52/53**, 169 (1983).
40. J. Murray and D. Hull, *Polymer,* **10,** 451 (1969).
41. D. Hull, *J. Mater. Sci.*, **5,** 357 (1970).

Received September 23, 1991
Accepted November 6, 1991